Optimization of the Plasma Response for the Control of Edge-Localized Modes with 3D Fields

C. Paz-Soldan 1), R. Nazikian 2), R.A. Moyer 3), J.D. Callen 4), T.E. Evans 1), N.M. Ferraro 2), N.C. Logan 2), B.C. Lyons 1), X. Chen 1), L. Cui 2), D. Eldon 1), M.E. Fenstermacher 5), A.M. Garofalo 1), B.A. Grierson 2), R.J. Groebner 1), C.C. Hegna 4), S.R. Haskey 2), M.J. Lanctot 1), C.J. Lasnier 5), T.C. Luce 1), G.R. McKee 4), D. Orlov 3), T.L. Rhodes 6), M.W. Shafer 7), P.B. Snyder 1), W.M. Solomon 1), E.J. Strait 1), R.S. Wilcox 7), A. Wingen 7)

1) General Atomics, San Diego, CA 92186-5608, USA
2) Princeton Plasma Physics Laboratory, Princeton, New Jersey 08543-0451, USA
3) University of California-San Diego, La Jolla, CA 92093-0417, USA
4) University of Wisconsin-Madison, Madison, WI 53706-1609, USA
5) Lawrence Livermore National Laboratory, Livermore, California 94550, USA
6) University of California-Los Angeles, Los Angeles, CA 90095, USA
7) Oak Ridge National Laboratory, Oak Ridge, TN 37831, USA

e-mail contact of main author: paz-soldan@fusion.gat.com

Abstract. Measurements and modeling of the plasma response to applied 3D magnetic perturbations - specifically its dependence on collisionality, beta, and rotation - yield new insights into the physics of edge-localized mode (ELM) control and better define the criteria needed to achieve ELM suppression in ITER. ELM control depends on the coupling of the applied field to a stable edge mode that drives resonant fields on edge rational surfaces and is directly observed on high-field side (HFS) magnetic sensors. The edge mode amplitude is inversely proportional to pedestal collisionality yet is insensitive to global beta, consistent with a current-driven mode as opposed to a pressure-driven kink, and reinforcing the importance of ITER-like collisionality for driving resonant fields. Onset of ELM-suppression is consistent with a transport bifurcation driven by the penetration of resonant fields, evidenced by sudden changes in: boundary heat flux, pedestal-top rotation and fluctuations, and HFS magnetic effects. Systematic torque scans reveal a loss of ELM suppression at low torque consistent with two-fluid modeling predictions of a reduction in the penetrated field. These results point to the need to control the equilibrium profiles to optimize the plasma response for ELM control in ITER.

1. Introduction and Motivation

Improvements in measurement and modeling of the plasma response to applied 3D magnetic perturbations on DIII-D demonstrate how to optimize the applied 3D spectrum and axi-symmetric equilibrium conditions to achieve ELM suppression in ITER. Plasma response effects can determine whether or not ELMs are suppressed, even when the magnitude of the applied 3D perturbations is above usual threshold values. Figure 1 displays two 15 MA Qivalent DIII-D pulses (ITER shape, I/aB = 1.4, β_N= 2) - one with all co-I_P directed neutral beam (NBI) torque (T_{NBI}) and another with added counter-I_P directed T_{NBI}. Despite the ITER design criteria for ELM suppression (vacuum island overlap width $> 16.5\%$) being exceeded in both plasmas, ELM suppression is not successful at low rotation. This highlights the crucial role of plasma response and especially the plasma rotation to the control of ELMs with 3D fields. These effects will be discussed herein.

DIII-D experiments are identifying the conditions associated with access to ELM suppression as well as the underlying physics behind the transition into the ELM-suppressed state, both in ITER 15 MA Q=10 equivalent pulses and beyond. Varying the applied poloidal spectrum of n=2 perturbations by slowly scanning the phase difference between upper and lower coils ($\Delta\phi_{UL}$) reveals ELM suppression occurs at the peak of the 'tearing drive'[1] as calculated by the Ideal Perturbed Equilibrium Code (IPEC).[1] When tearing drive is maximized (Fig. 2), a swift bifurcation in the pedestal conditions is observed - evidenced most prominently by a sudden increase in the toroidal rotation and the magnetic response measured on recently installed high-field side (HFS) sensors.[2]

These observations form the structure for this work. First, the optimization of the tearing drive is discussed. Tearing drive can be maximized both by optimizing the structure of the applied 3D perturbations as well as optimizing the axisymmetric equilibrium conditions. Second, bifurcation observations will be shown to be consistent with resonant field penetration at an edge rational surface - the combination of large tearing drive together with low electron rotation ($\omega_{\perp,e}$) at the rational surface. Third, optimizing the $\omega_{\perp,e}$ profile to enable penetration at the resonant surface will be discussed. Discussion of the extrapolation to ITER conditions and bifurcation model development concludes this work.

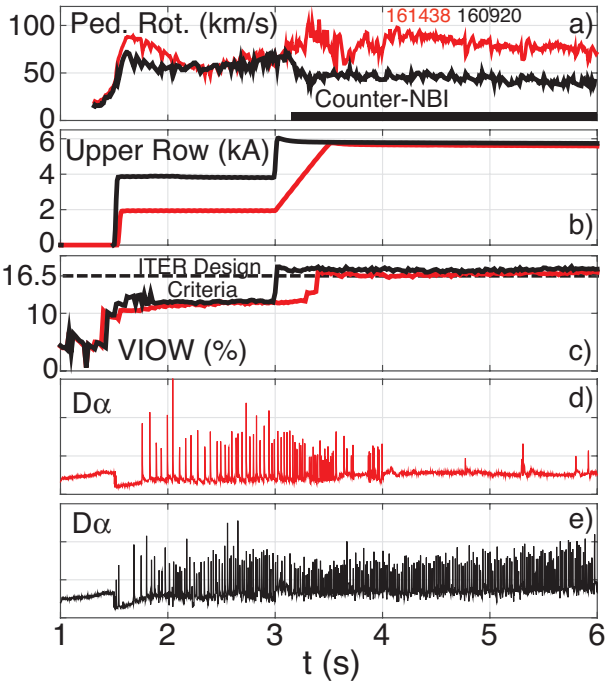

FIG. 1. Discharges with similar pedestal conditions and applied field strength (quantified by vacuum island overlap width, VIOW) yet different T_{NBI} and toroidal rotation. ELMs in the lower rotation discharge are not suppressed.

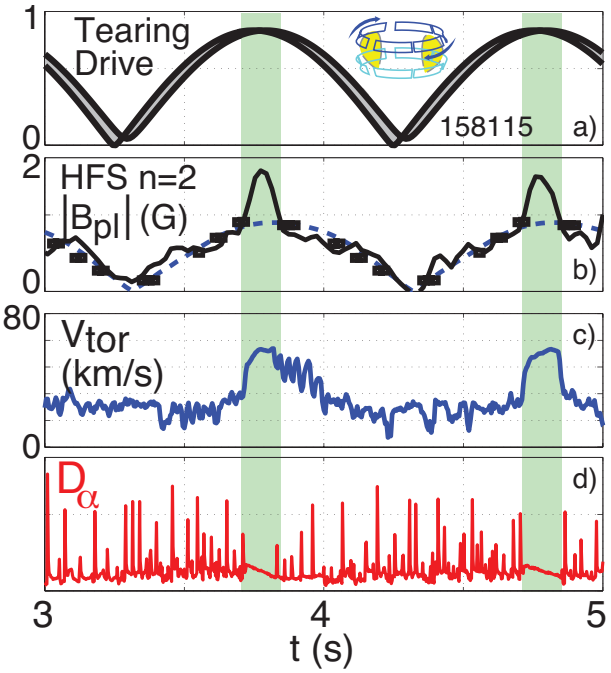

FIG. 2. Variation of the n=2 spectrum modulates the strength of the tearing drive. ELM suppression is found at the tearing drive peak and is coincident with an increase in the toroidal rotation and HFS magnetic response (B_{pl}).

[1]Tearing drive is defined in IPEC as the magnitude of the singular current (J_{res}) at a rational surface needed to maintain the ideal MHD constraint. In MARS-F non-ideal effects are included thus allowing finite resonant field penetration (B_{res}) whose magnitude represents the magnetic response to the tearing drive. M3D-C1 uses the same definition as MARS-F, though M3D-C1 can include two-fluid effects.

2. Optimization of the MHD Modal Response for Tearing Drive

The parametric dependencies of the tearing drive and how to optimize it with both the applied 3D spectrum and the axisymmetric equilibrium conditions is now discussed.

A Effect of Edge Safety Factor

A simple parametric dependency is the edge safety factor, q_{95}. Varying the equilibrium field-line pitch modifies the coupling to the resonant surfaces through modification of the poloidal mode structures excited within the plasma. These effects are taken into account in MARS-F modeling shown in Fig. 3, where q_{95} scaled equilibria are used to compute the optimal $\Delta\phi_{UL}$ to maximize the tearing drive. As shown, the optimal $\Delta\phi_{UL}$ is a sensitive function of q_{95}. Furthermore, the co-alignment of the HFS magnetic response (B_{pl}) and the tearing response (B_{res}) shown in Fig. 2 is reproduced across q_{95}, though a higher order variation is also found. The low-field side (LFS) plasma response is also consistently maximized at a different $\Delta\phi_{UL}$ than the tearing drive and HFS response, indicating different plasma response modes are acting on each.[3]

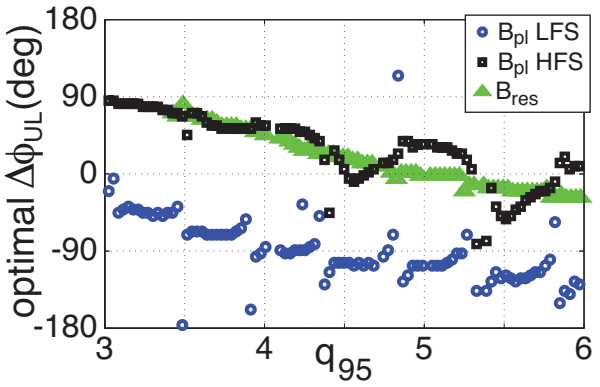

FIG. 3. MARS-F calculation of optimal n=2 $\Delta\phi_{UL}$ to maximize the tearing response (B_{res}) and magnetic response (B_{pl}) as q_{95} is varied.

B Effect of Plasma Beta and Collisionality

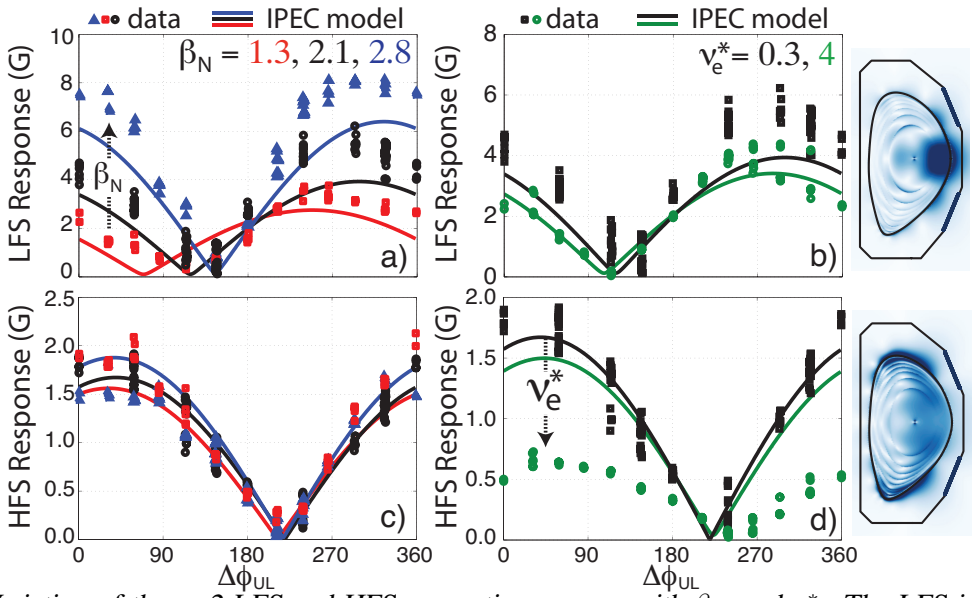

FIG. 4. Variation of the n=2 LFS and HFS magnetic response with β_N and ν_e^*. The LFS is primarily sensitive to β_N while the HFS is primarily sensitive to ν_e^*. Note the HFS response extends to the top and bottom of the device as shown in the cross-section inset.

The effect of global average plasma pressure (β_N) and pedestal collisionality (ν_e^*) are considered experimentally and computationally. Measurements (shown in Fig. 4) of the n=2 magnetic plasma response are made on the LFS and HFS as β_N and ν_e^* are varied by changing NBI

power at fixed ν_e^* and density at fixed β_N respectively.[3] Note ρ_* also varied in these scans. Experiment clearly indicates that the LFS response is sensitive to β_N, and only weakly to ν_e^*. On the HFS, the opposite trend is found - with strong sensitivity to ν_e^* and only weak sensitivity to β_N. The same trend is found at all $\Delta\phi_{UL}$ considered. Ideal MHD modeling of experimental trends is done with scaled equilibria (shown in Fig. 5), with the β_N scan modeled by changing the core β_N without changing $\beta_{N,ped}$ and the ν_e^* scan modeled by varying J_{boot} at constant β_N. IPEC modeling (Fig 4) captures both LFS trends very well, and also the invariance of the HFS response with β_N. However, the strong experimental dependence of the HFS response with J_{boot} (ν_e^*) is not reproduced in IPEC. Resistive MARS-F results are very similar to IPEC. The reason for the disagreement in the HFS response with ν_e^* appears to be due to subtleties in the edge current profile and separatrix treatment and is still under investigation.[3]

Scaled equilibria are also used to assess the dependence of the tearing drive on equilibrium conditions, as shown in figure 6. The core β_N drive is found to increase coupling to the core resonant surfaces, but has only a weak or even negative effects on the tearing drive of the edge rational surfaces. Thus, despite the stronger instability drive at high core β_N, this drive does not translate into a beneficial increase in edge tearing drive. In contrast, scaled equilibria with larger J_{boot} are found to have increased tearing drive and response at edge surfaces, with little change in the core. This result mirrors the LFS and HFS plasma response differences found in Fig. 4. The HFS response thus experimentally displays the same trends in β_N, ν_e^*, and q_{95} as the pedestal-top tearing drive.

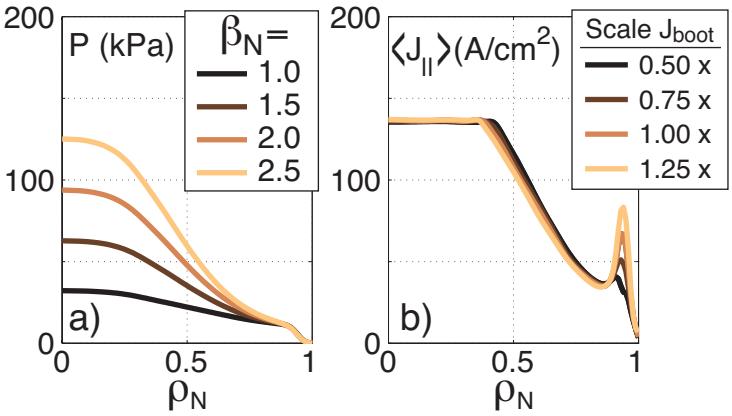

FIG. 5. Scaled equilibria used to assess trends in tearing drive with β_N and J_{boot}.

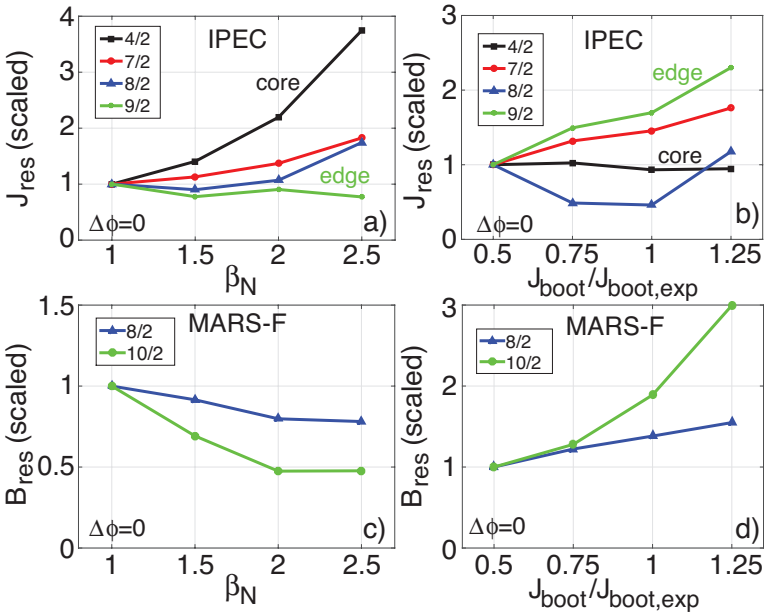

FIG. 6. Scaling of tearing drive in IPEC (resonant current, J_{res}) and MARS-F resonant response (B_{res}) as core β_N and J_{boot} are scanned in scaled equilibria. J_{res} and B_{res} is found to depend more on J_{boot} than core β_N.

C Shielding and Amplifying Modes

The results of Fig. 4 indicate that though the experimental HFS response does depend on ν_e^*, the IPEC computed HFS response is insensitive to both pressure and current profile - the only instability drives of ideal MHD. This led to a theoretical study to identify highly stable plasma response modes that may still play a role in the pedestal. The result was a new appreciation of the plasma reluctance and a path to drive tearing with minimal impact on global stability.[4] The plasma reluctance is a Hermetian basis to describe the MHD mode spectrum, ranked by a given mode's ability to drive perturbed current $\tilde{I}_p$ from an imposed external flux Φ_x (Fig. 7[a]). This is given by the matrix relation: $\tilde{I}_p = \rho\Phi_x$, where ρ is the reluctance matrix. Sorting modes in this basis by taking the eigenvectors and eigenvalues of the reluctance results in a separation of reluctance modes into "shielding" and "amplifying" modes - differentiated by the sign of the reluctance eigenvalue. Positive reluctance modes add to the applied perturbed field (thus amplifying it), while negative reluctance modes subtract (and thus shield). Further, the amplifying modes are LFS localized while the shielding modes have strong contributions on the HFS (Fig. 7[b,c]). Considering the contribution to the perturbed energy (δW) of each reluctance mode, it is found that amplifying modes are the least stable (smallest δW) and shielding modes are the most stable (largest δW) (Fig. 7[d]). In addition to the well-known ability of amplifying modes to contribute to the tearing drive, the stable shielding modes are also shown to be able to contribute to the tearing drive (Fig. 7[e]). As each reluctance mode is orthogonal, a suitably chosen Φ_x can only couple to the stable shielding modes. This shows a path to ELM control with large tearing drive yet minimal impact on instability through δW.

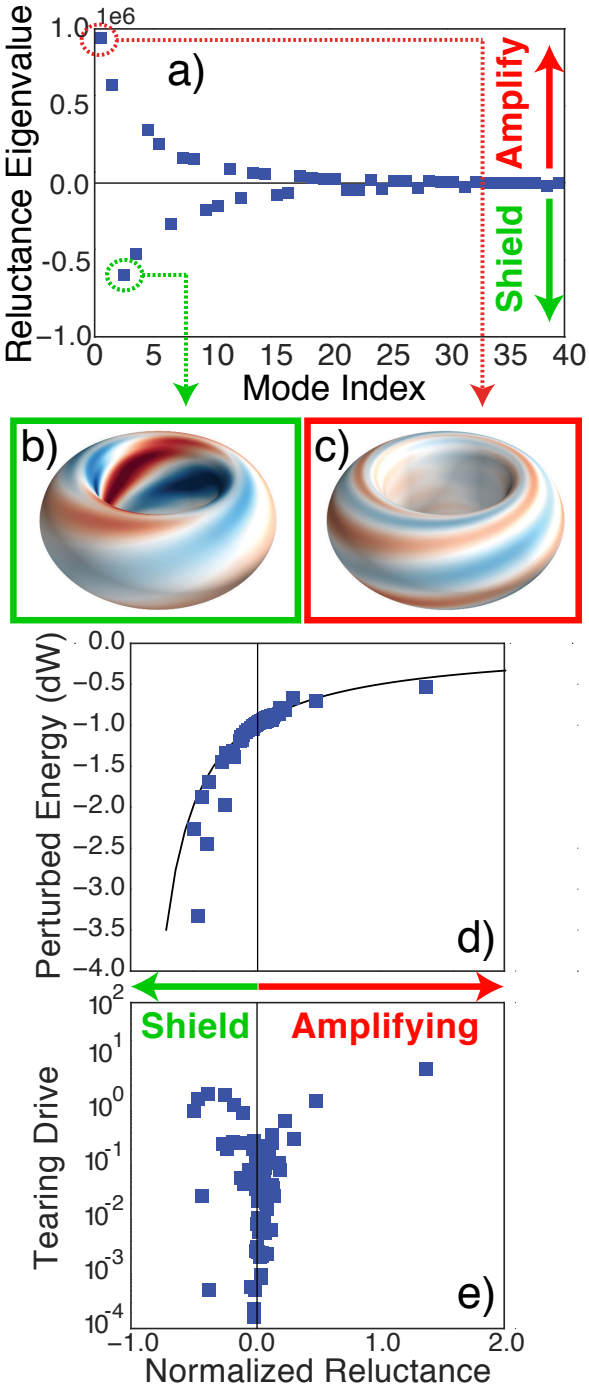

FIG. 7. Mode structure (b,c) and stability (d) of reluctance Eigenmodes for the discharge of Fig. 2. Negative reluctance modes are most stable, have significant amplitude on the HFS side, and can drive tearing. Positive reluctance Eigenmodes are LFS localized, least stable, and can also drive tearing.

3. Consistency of Pedestal Bifurcation with Field Penetration

Once tearing drive is sufficiently strong, bifurcations into the ELM-suppressed state are observed. The clearest indications of bifurcation are in the toroidal rotation and the HFS magnetic response. These effects are now considered systematically with single-fluid M3D-C1 modeling. In single-fluid MHD, the ExB rotation (ω_E) takes the place of $\omega_{\perp,e}$ as the relevant rotation for field penetration. Figure 8 displays the reconstructed profiles of ω_E in and out of ELM suppression, for rotation profiles measured immediately before and 50 ms after a bifurcation like the one shown in Fig. 2. Due to the role of the diamagnetic flows, the increase in toroidal rotation (Fig. 2) is coincident with a movement of the ω_E zero-crossing region from the 7/2 rational surface to the 8/2 rational surface. M3D-C1 modeling varying only the rotation profile indicates the rotation profile change should result in a vertical motion of the HFS magnetic response pattern with an associated toroidal phase shift, consistent with the dominant poloidal mode number switching from odd to even.[5] This occurs together with a shift in the location of maximum penetration from the 7/2 to the 8/2 surface.

This prediction is experimentally verified at the exact moment the plasma back-transitions from ELM suppression to ELM-free (yet preceding the ELM itself), as shown in Fig. 9 at 2.10 s. The back-transition to ELM-free behavior is characterized by a simultaneous drop in the D_α baseline, an increase in $T_{e,ped}$, and a reduction of density fluctuations at the top of the pedestal. Examination of the HFS plasma response at the instant of back-transition reveals the expected change in the HFS response - a vertical motion and toroidal phase shift of the helical structures - as expected for a change in field penetration at the 8/2 surface.

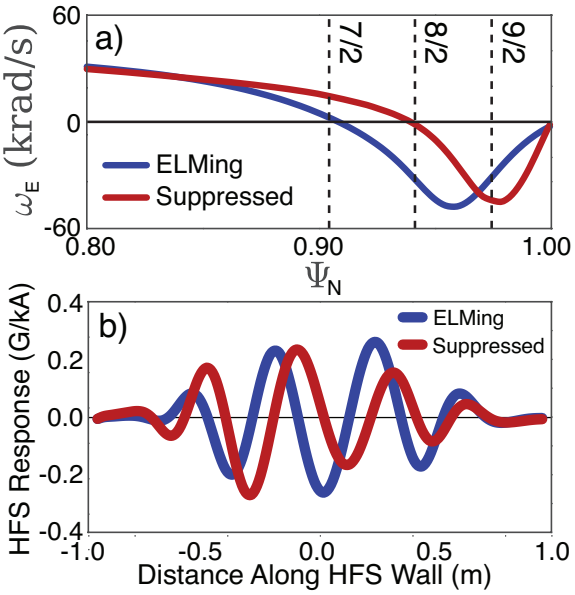

FIG. 8. Variation of rotation profile in and out of ELM suppression. A vertical shift in the M3D-C1 predicted HFS response structure occurs when field penetration moves to the 8/2 surface.

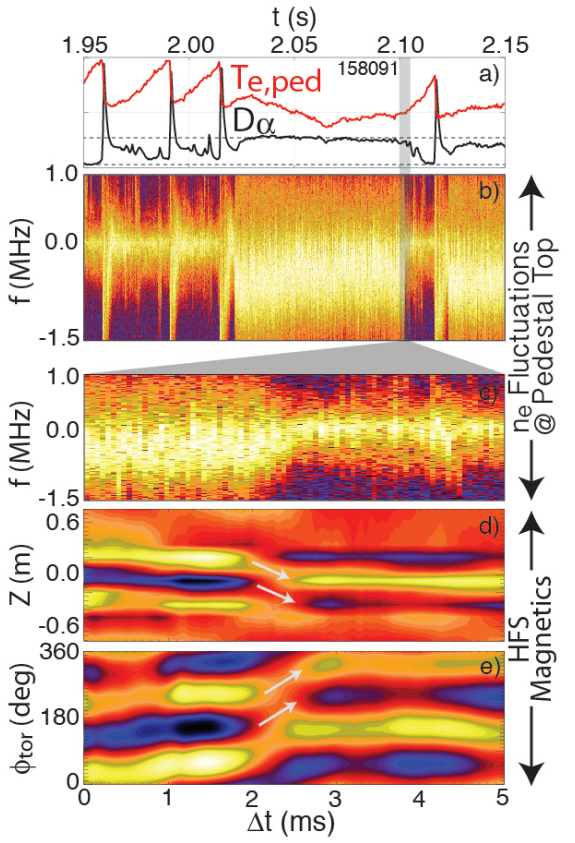

FIG. 9. Experimental observation of back-transition from ELM suppressed to ELM-free occurs with a sharp transition in the density fluctuations and the HFS magnetic response.

4. Optimization of the Tearing Layer Response

The previous sections described how maximal tearing drive together with low $\omega_{\perp,e}$ at the rational surface combine to allow field penetration and control of ELMs. However, low $\omega_{\perp,e}$ at an edge rational surface is not guaranteed, and $\omega_{\perp,e}$ control is necessary to optimize the layer response and allow field penetration.

A Performance Recovery

While initial application of 3D fields often degrades performance through the 'density pumpout' effect, the non-linearity of field penetration gives rise to hysteresis effects that allow confinement to be regained until the plasma back-transitions out of ELM suppression. Figure 10 demonstrates the effect of first increasing the n=3 RMP magnitude to access ELM suppression at lower confinement, but then reducing the RMP magnitude until ELM suppression is lost. As RMP magnitude is slowly reduced the plasma confinement reaches the pre-RMP level, yet the plasma is maintained in the ELM suppressed state. Examination of the pedestal profiles (Fig 10[d,e]) indicate that despite the increase in core toroidal rotation and pressure, gradient driven flows in the pedestal-top region maintain low $\omega_{\perp,e}$ at the edge rational surface. This shows that a wide variety of pedestal profiles can be consistent with low $\omega_{\perp,e}$ at the rational surface, and that the pedestal can be optimized maintaining an $\omega_{\perp,e}$=0 constraint.

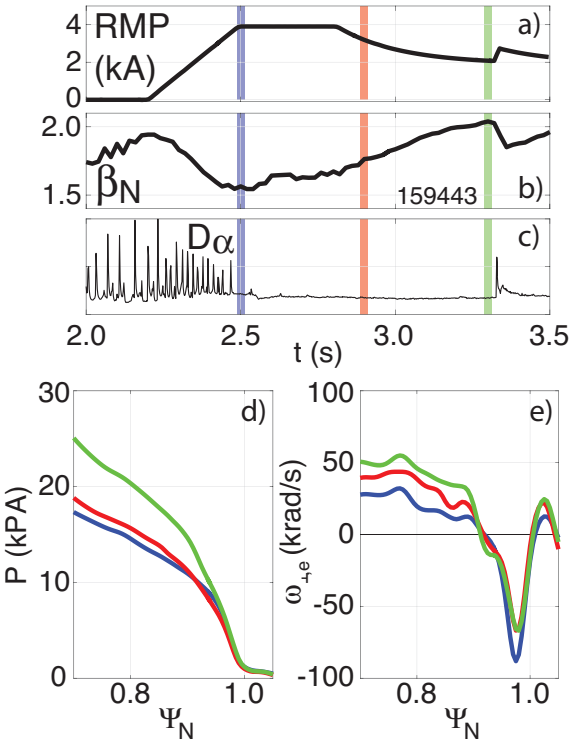

FIG. 10. Performance recovery after entry to n=3 ELM suppression is enabled by reducing RMP coil magnitude and employing hysteresis in the back-transition. Input power is constant throughout.

B Effect of NBI Torque

Variation of T_{NBI} can alter the inner boundary condition for the toroidal rotation and thus modify the torque balance at the rational surface. Figure 11 demonstrates this effect with n=3 fields, where increasing T_{NBI} from 3.5 to 5 Nm at 4.5 s increases edge rotation, and brings

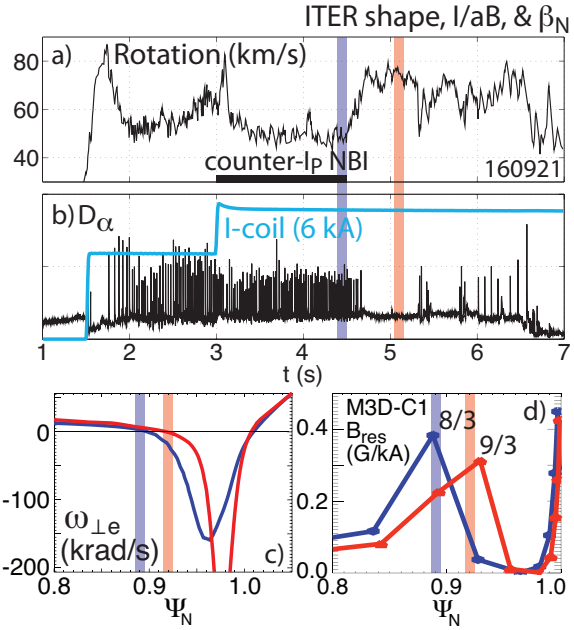

FIG. 11. Increase of toroidal rotation through increasing T_{NBI} accesses ELM suppression. The $\omega_{\perp,e}$ zero crossing and subsequent field penetration moves from the 8/3 to the 9/3 surface when T_{NBI} is increased.

the plasma into ELM suppression.[6] This is coincident with the low $\omega_{\perp,e}$ region going from the 8/3 to the 9/3 surface, and thus field penetration is computed to occur at the 9/3 surface. This could be overcome by either increasing the tearing drive (and local torque) at the 9/3 surface or manipulating the diamagnetic flow profile to reduce $\omega_{\perp,e}$, as changes to the pedestal structure and diamagnetic flows which also enter into $\omega_{\perp,e}$.

5. Conclusion and Extrapolation

DIII-D experiments demonstrate the crucial importance of sufficiently large tearing drive together with low $\omega_{\perp,e}$ on edge rational surfaces for ELM suppression (Fig. 2).[1, 2] HFS magnetic sensors are sensitive to penetration of pedestal top resonant fields (Fig. 9) and are well-modeled with the IPEC and MARS-F codes (Figs. 4 & 8), except for the experimental ν_e^* dependence.[3] Scaling studies highlight key dependencies of the tearing drive (J_{res}) and response (B_{res}) on q_{95}, J_{boot}, and β_N (Fig. 3 & 6). The plasma reluctance [4] offers a methodology (Fig. 7) to maximizing the tearing drive without detrimentally affecting stability (δW). Tearing drive can thus be optimized by matching $\Delta\phi_{UL}$ to a given q_{95}, accessing low ν_e^*, and preferentially exciting negative reluctance modes. Even with large tearing drive, changes in $\omega_{\perp,e}$ can prevent penetration of resonant fields and cause loss of ELM suppression, as occurs with the addition of counter-I_P T_{NBI} (Fig. 1 & 11). ω_E and $\omega_{\perp,e}$ rotation are low at rational surfaces in ELM-suppressed states (Fig. 8) but the relation of this to rotation actuators (RMP, intrinsic, and NBI) is not yet clear. Diamagnetic flow profiles can also be optimized to allow low $\omega_{\perp,e}$ at the rational surface. Finally, access to ELM suppression is a non-linear process and can be precipitated by an ELM crash that transiently lowers rotation and increases tearing drive. A model for this process and its dependence on plasma rotation at the rational surface is just beginning to be explored.[7]

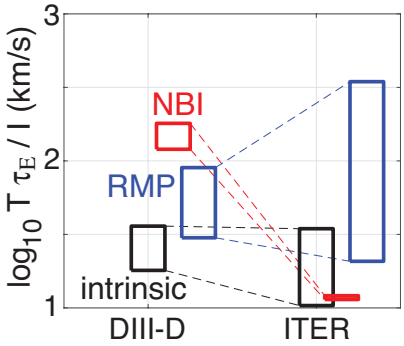

FIG. 12. Expected 0-D scaled rotation (torque × confinement time / moment of inertia) from DIII-D to ITER.

The primary implications of these results for ITER are: 1) maximizing the tearing drive by optimizing the applied spectrum and equilibrium parameters will yield the highest likelihood of ELM suppression, and 2) how the possible plasma rotation actuators influence the bifurcation into the ELM-suppressed state require further study since their relative contribution to ITER rotation will be different (Fig. 12). DIII-D data shown in this paper can be obtained in digital format by following the links at https://fusion.gat.com/global/D3D_DMP. Work supported by US DOE under DE-FC02-04ER54698.

References

[1] C. Paz-Soldan et al, Phys. Rev. Lett. 114, 105001 (2015).
[2] R. Nazikian et al, Phys. Rev. Lett. 114, 105002 (2015).
[3] C. Paz-Soldan et al, Nucl. Fusion 56, 056001 (2016).
[4] N.C. Logan et al, Phys. Plasmas 23, 056110 (2016).
[5] B.C. Lyons et al, submitted to Plasma Phys. Contrl. Fusion (2016).
[6] R.A. Moyer et al, Phys. Plasmas (2017, in preparation).
[7] J.D. Callen et al, Plasma Phys. Contrl. Fusion (2017, in preparation).